Stability Analysis of a Non-Inverting Synchronous Buck-Boost Power Converter for a Solar Power Management System

Jaw-Kuen Shiau, *Member, IEEE*, Chun-Jen Cheng, and Ching-En Tseng

***Abstract*: This paper presents the stability analysis of a non-inverting synchronous buck-boost DC/DC power converter for a solar power management system. The system can operate in buck, buck-boost or boost mode according to the condition of the supply voltage. The variation of the supply voltage arises from the rapid changes of the atmospheric condition or sunlight incident angle. The stability margins of each individual operation mode for different system parameters (inductor, capacitor) and load conditions are analyzed first. The results show that the stability margins depend on the inductor and capacitor selected for the converter and depend on the load conditions also. The systems are then modeled as Markov jump systems for evaluating the mean square stability of the systems. With careful selection of the system parameters, adequate stability margins of each individual operation mode and mean square stability of the jump system can be assured. The buck-boost converter is incorporated into the solar power battery management system to maximize the utility of the available solar power drawn from the solar panel.**

I. INTRODUCTION

Solar powers are widespread in industry, commercial, and military applications [1-3]. A typical DC type solar power management system is shown in Figure 1[4]. It contains maximum power point tracking, battery management (energy storage), and power conversion stages. Each stage requires certain types of power converters. Due to a possible rapid variation of the acquired solar power (changes of the atmospheric condition, or sunlight incident angle), a buck-boost type DC/DC converter is desired for the battery management system to maximize the utility of the solar power. Figure 2 shows the results of power variation due to rapid changes of the atmospheric conditions. The test was conducted at Tamkang University using the natural sunlight as the irradiation source. In this study, the input the buck-boost power converter system for the battery management is considered to be varying from 6 to 30 volts. The output of the converter is regulated to 12.6 V to charge the Li-ion battery modules.

Analysis and design of buck-boost power converters are widely studied recently [5-8]. The buck-boost converters presented in [6,7] are for portable applications. In [8], a buck-boost cascaded converter is proposed for high power applications such as fuel cell electric vehicles. In this paper we concentrate on small signal stability analysis of buck-boost power converter. The converter will jump among the buck, buck-boost, and boost operation modes according to the variations of the input supply voltage. The stability margins for the converter system with various system parameters and load conditions for each operation mode are evaluated. We also model the small signal dynamic systems as a Markov jump linear system to assess the mean square stability of the jump system. Application of the buck-boost power converter to a solar power battery management system is also discussed in the paper.

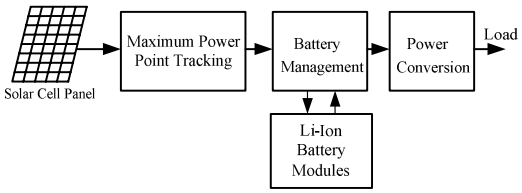

Figure 1. Configuration of the solar power management system

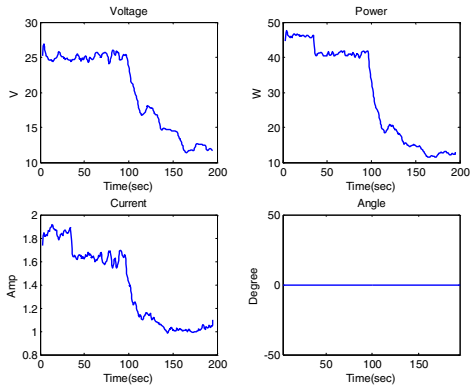

Figure 2. Solar power variations due to rapid changes of the atmosphere condition

II. SYNCHRONOUS BUCK-BOOST CONVERTER BACKGROUND

The non-inverting buck-boost converter is capable of converting the source supply voltage to higher and lower voltages to the load terminal with voltage polarity unchanged. A schematic of the synchronous buck-boost circuit is shown in Figure 3. Four high speed power MOSFETs are employed to control the energy flow from the supply to the load terminal.

Manuscript received June 10, 2008.

Jaw-Kuen Shiau is with the Department of Aerospace Engineering, Tamkang University, Tamsui, TAIWAN,25137 (phone:886-2-26215656 ext 3318, fax:886-2-26209746, email:shiauj@mail.tku.edu.tw).

Chun-Jen Cheng is currently working toward his MS degree at the Department of Aerospace Engineering, Tamkang University.

Ching-En Tseng is currently working toward his Ph.D. degree at the Department of Mechanical Engineering, National Taiwan University, Taipei, TAIWAN.

978-1-4244-1888-6/08/$25.00 ©

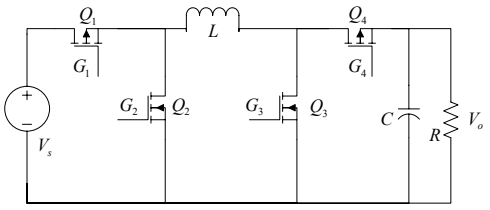

Figure 3. Synchronous non-inverting buck-boost power converter

Due to variations of the supply voltage, the power converter is able to operate in buck, buck-boost, or boost mode through properly control of the power MOSFETs. When the supply voltage is higher than the desired load voltage, the converter is set up for buck operation. In buck mode operation, the transistor Q_4 is always on and Q_3 is always off. The simplified equivalent circuitries of the power converter for inductor charge and discharge in buck operation is shown in Figure 4. In Figure 4(a), the transistor Q_1 is closed while Q_2 is open, thus the supply voltage charges the inductor. In inductor charging cycle, the inductor current will increase nearly linearly and the capacitor will supply output current (i.e., in discharging state) to the load R . In Figure 4(b), we close the transistor Q_2 , and open the transistor Q_1 to engage the inductor discharge mode. In this mode, the energy stored in the inductor will be delivered to the capacitor (charging the capacitor) and the load. The current from the inductor will decrease nearly linearly during the inductor discharge period. In this mode, the average load voltage v_O is equal to Dv_S , where D is the duty cycle.

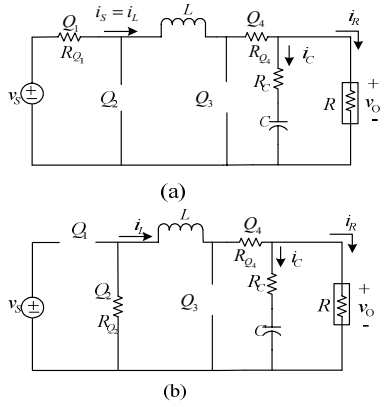

Figure 4.Buck Mode Operation (a) Inductor charge (b) Inductor discharge

When the supply voltage is lower than the desired load voltage, the converter is set up for boost operation. In boost mode operation, the transistor Q_1 is always on and Q_2 is always off. The simplified circuitries of the power converter for inductor charge and discharge in boost operation is shown in Figure 5. In Figure 5(a), the transistor Q_3 is closed while Q_4 is open, thus the supply voltage charges the inductor. In Figure 5(b), we close the transistor Q_4 , and open the transistor Q_3 to engage the inductor discharge mode. In this mode, the average load voltage v_O is equal to $v_S/(1-D)$, where D is the duty cycle.

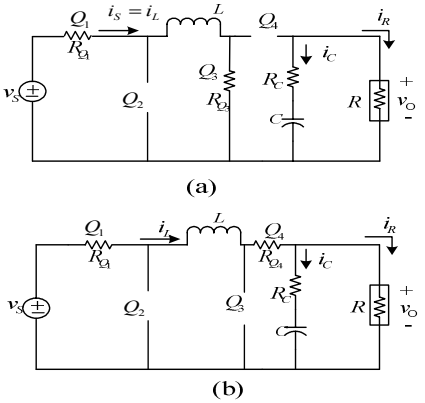

Figure 5. Boost Mode Operation (a) Inductor charge (b) Inductor discharge

When the supply voltage is close to the desired load voltage, the converter is set up for buck-boost operation. The transistors Q_1 and Q_3 work as one group and Q_2 and Q_4 work as another group. The simplified equivalent circuits at different operating modes are shown in Figure 6. In Figure 6(a), the transistors (the switches) Q_1 and Q_3 are closed, while Q_2 and Q_4 are open, thus the supply voltage charges the inductor. In Figure 6(b), we close the transistors Q_2 and Q_4 , and open the transistors Q_1 and Q_3 to engage the inductor discharge mode. In this mode, the average load voltage v_O is equal to $v_S D/(1-D)$.

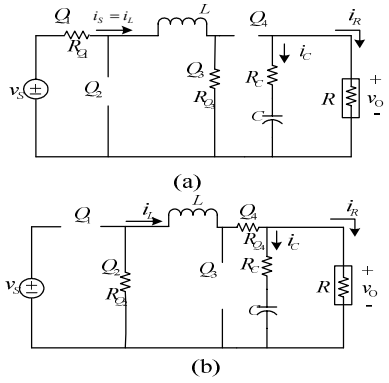

Figure 6. Buck-Boost Mode Operation (a) Inductor charge (b) Inductor discharge

III. DYNAMIC CHARACTERISTICS

To provide a good voltage regulation of the power converter, stability analysis for duty-cycle variations are

conducted in this research. The dynamical equations of the power converter can be derived by using the state-space averaging techniques. The small signal models are obtained by applying a small perturbation to the system, and neglect the second order terms. The small signal dynamical model for the buck mode operation is

$$\begin{bmatrix} \frac{d\tilde{i}_L}{dt} \\ \frac{d\tilde{v}_C}{dt} \end{bmatrix} = \begin{pmatrix} \frac{R_{T1}}{L(R+R_C)} & -\frac{R}{L(R+R_C)} \\ \frac{R}{C(R+R_C)} & -\frac{1}{C(R+R_C)} \end{pmatrix} \begin{bmatrix} \tilde{i}_L \\ \tilde{v}_C \end{bmatrix} + \begin{bmatrix} \frac{D}{L} \\ 0 \end{bmatrix} \tilde{v}_S + \begin{pmatrix} \frac{R_{T2}I_L + V_S(R+R_C)}{L(R+R_C)} \\ 0 \end{pmatrix} \tilde{d} \quad (1)$$

$$\tilde{v}_O = \begin{pmatrix} \frac{RR_C}{(R+R_C)} & \frac{R}{(R+R_C)} \end{pmatrix} \begin{pmatrix} \tilde{i}_L \\ \tilde{v}_C \end{pmatrix} \quad (2)$$

$$R_{T1} = DR_{D1} + D'R_{D2}, R_{T2} = R_{D1} - R_{D2}$$

$$R_{D1} = -(R_{Q_1} + R_{Q_3})(R+R_C) - RR_C \quad , R_{D2} = -(R_{Q_2} + R_{Q_4})(R+R_C) - RR_C$$

$d = D + \tilde{d}$, $d' = D' - \tilde{d}$, $v_S = V_S + \tilde{v}_S$, $i_L = I_L + \tilde{i}_L$, $v_O = V_O + \tilde{v}_O$, where D , $D' = 1 - D$, V_S , I_L , and V_O represent the system parameters under steady state conditions.

The small signal dynamical model for the boost mode operation is

$$\begin{bmatrix} \frac{d\tilde{i}_L}{dt} \\ \frac{d\tilde{v}_C}{dt} \end{bmatrix} = \begin{pmatrix} \frac{R_{T1}}{L(R+R_C)} & -\frac{D'R}{L(R+R_C)} \\ \frac{D'R}{(R+R_C)C} & -\frac{1}{C(R+R_C)} \end{pmatrix} \begin{bmatrix} \tilde{i}_L \\ \tilde{v}_C \end{bmatrix} + \begin{bmatrix} \frac{1}{L} \\ 0 \end{bmatrix} \tilde{v}_S + \begin{pmatrix} \frac{R_{T2}I_L + RV_C}{L(R+R_C)} \\ -\frac{RI_L}{C(R+R_C)} \end{pmatrix} \tilde{d} \quad (3)$$

$$\tilde{v}_O = \begin{pmatrix} \frac{D'RR_C}{(R+R_C)} & \frac{R}{(R+R_C)} \end{pmatrix} \begin{pmatrix} \tilde{i}_L \\ \tilde{v}_C \end{pmatrix} + (-\frac{RR_CI_L}{(R+R_C)})\tilde{d} \quad (4)$$

$$R_{T1} = DR_{D1}(R+R_C) + D'R_{D2} \ , \ R_{T2} = R_{D1}(R+R_C) - R_{D2}$$

$$R_{D1} = -(R_{Q_1} + R_{Q_3}) \ , \ R_{D2} = -(R_{Q_1} + R_{Q_4})(R+R_C) - RR_C$$

The small signal dynamical model for the buck-boost mode operation is

$$\begin{bmatrix} \frac{d\tilde{i}_L}{dt} \\ \frac{d\tilde{v}_C}{dt} \end{bmatrix} = \begin{pmatrix} \frac{R_{T1}}{L(R+R_C)} & -\frac{D'R}{L(R+R_C)} \\ \frac{D'R}{C(R+R_C)} & -\frac{1}{C(R+R_C)} \end{pmatrix} \begin{bmatrix} \tilde{i}_L \\ \tilde{v}_C \end{bmatrix} + \begin{bmatrix} \frac{D}{L} \\ 0 \end{bmatrix} \tilde{v}_S + \begin{pmatrix} \frac{R_{T2}I_L + RV_C + V_S(R+R_C)}{L(R+R_C)} \\ -\frac{RI_L}{C(R+R_C)} \end{pmatrix} \tilde{d} \quad (5)$$

$$\tilde{v}_O = \begin{pmatrix} \frac{D'RR_C}{(R+R_C)} & \frac{R}{(R+R_C)} \end{pmatrix} \begin{pmatrix} \tilde{i}_L \\ \tilde{v}_C \end{pmatrix} + (-\frac{RR_CI_L}{(R+R_C)})\tilde{d} \quad (6)$$

$$R_{T1} = DR_{D1}(R+R_C) + D'R_{D2} \ , R_{T2} = R_{D1}(R+R_C) - R_{D2}$$

$$R_{D1} = -(R_{Q_1} + R_{Q_3}), \ R_{D2} = R^2 - (R+R_C)(R_{Q_2} + R_{Q_4} + R)$$

The system characteristic depends on the inductor inductance and capacitor capacitance. The factors which need to be considered for determining the inductance L include: the input voltage range, the output voltage, the inductor current, the switching frequency, and so on. The capacitor is used to maintain a well-regulated voltage. The capacitance depends on the inductor current ripple, the switching frequency, and the desired output voltage ripple. In this design, the input voltage is considered to be varied from 6 to 30 volts. The load voltage is to be regulated at 12.6 V. When the supply voltage is higher than 13.4 V, we will set the converter to operate in buck mode. If the supply voltage is below 11.84 V, we set the power converter to operate in the boost mode. When the supply voltage falls within 11.84 and 13.4 volts, the converter is set to operate in buck-boost mode. With 300 kHz switching frequency, 3A output current, 40% maximum inductor current ripple, and 0.02V output voltage ripple, the inductor and capacitor values are selected as $L = 21\ \mu\text{H}$, and $C = 470\ \mu\text{F}$. The stability margins of the system from duty cycle variations $\tilde{d}$ to output voltage variations $\tilde{v}_O$ with respect to the supply voltage variations are shown in Figure 7. The results are summarized in Table 1. In Figure 7, the results for 1A and 0.1A loads are also included. The stability margins will be improved when the load current is reduced.

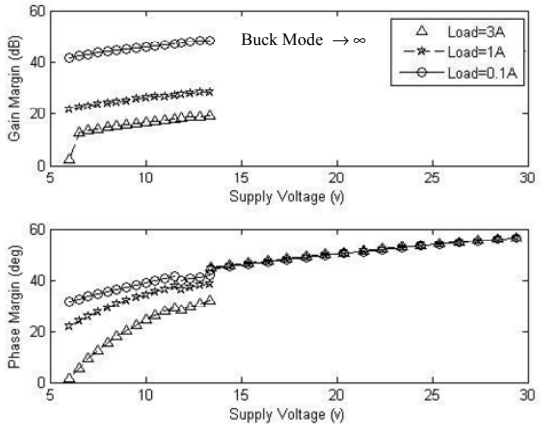

Figure 7. Stability Margins of the Buck-Boost Power Converter System $L = 21\mu\text{H},\ C = 470\mu\text{F}$

Table 1: Summaries of the Stability Margins ($L = 21\mu\text{H},\ C = 470\mu\text{F}$ with 3A load)

	Gain Margin	Phase Margin
Buck (13.4~30V)	∞	44.78~56.94
Buck-Boost (11.84V~13.4V)	17.96~18.99	28.49~32.08
Boost (6V~11.84)	2.29~17.92	1.605~30.05

When the inductor and capacitor values are selected with $L=15\mu\text{H},\ C=600\mu\text{F}$, the stability margins are shown in Figure 8. The results for 3A load are summarized in Table 2.

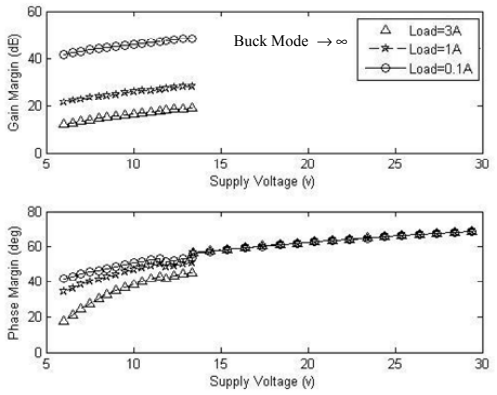

Figure 8. Stability Margins of the Buck-Boost Power Converter System for $L=15\mu\text{H},\ C=600\mu\text{F}$

Table 2. Summaries of the Stability Margins ($L=15\mu\text{H},\ C=600\mu\text{F}$, with 3A load)

	Gain Margin	Phase Margin
Buck (13.4~30V)	∞	56.4~68.52
Buck-Boost (11.84V~13.4V)	17.96~18.99	41.92~45.35
Boost (6V~11.84)	12.05~17.92	17.78~43.84

From the above results, the stability margins depend on the inductor and capacitor selected and the load condition. Besides, the system will jump among the three operation modes according to the condition of the supply voltage. The variation of the supply voltage arises from the rapid changes of the atmosphere conditions or the changes of the sunlight incident angles. Therefore, in addition to stability consideration for each individual operation mode, consideration for the mean square stability of the jump system is needed.

IV. MEAN SQUARE STABILITY ANALYSIS

The system will jump among the buck, buck-boost, and boost operation modes according to the conditions of the supply voltage. Considering the worst case condition (in the sense of stability margins), the state space models of the three modes can be written as

$$\begin{cases}\dot{x}=A_i x+B_i u\\ y=C_i x+D_i u\end{cases}\quad i=1,2,3 \tag{7}$$

where $x=\begin{bmatrix}\tilde{i}_L & \tilde{v}_C\end{bmatrix}^T$, $u=\tilde{d}$, $y=\tilde{v}_O$, and $i=1$ represents the buck mode, $i=2$ represents the buck-boost mode, and $i=3$ is for the boost mode. The system matrices for $L=21\mu\text{H},\ C=470\mu\text{F}$ with 3A load are as follows

Buck Mode:

$$A_1=\begin{bmatrix}-3791.55 & -47169.81\\ 2107.59 & -501.81\end{bmatrix},\quad B_1=\begin{bmatrix}638095.24\\ 0\end{bmatrix}$$
$$C_1=\begin{bmatrix}0.0396 & 0.9906\end{bmatrix},\quad D_1=0$$

Buck-Boost Mode:

$$A_2=\begin{bmatrix}-2818.83 & -22851.50\\ 1021.02 & -501.81\end{bmatrix},\quad B_2=\begin{bmatrix}1164172.86\\ -6728.61\end{bmatrix},$$
$$C_2=\begin{bmatrix}0.0192 & 0.9906\end{bmatrix},\quad D_2=-0.1265$$

Boost Mode:

$$A_3=\begin{bmatrix}-2803.23 & -22461.81\\ 1003.61 & -501.81\end{bmatrix},\quad B_3=\begin{bmatrix}636226.42\\ -13277.80\end{bmatrix},$$
$$C_3=\begin{bmatrix}0.0189 & 0.9906\end{bmatrix},\quad D_3=-0.2496$$

For comparison study, we also investigate the characteristics of the systems for $L=15\mu\text{H},\ C=600\mu\text{F}$ with 3A load. The system matrices are as follows

Buck mode:

$$A_1=\begin{bmatrix}-5308.18 & -66037.74\\ 1650.94 & -393.08\end{bmatrix},\quad B_1=\begin{bmatrix}893333.33\\ 0\end{bmatrix}$$
$$C_1=\begin{bmatrix}0.0396 & 0.9906\end{bmatrix},\quad D_1=0$$

Buck-Boost Mode:

$$A_2=\begin{bmatrix}-3946.35 & -31992.09\\ 799.80 & -393.08\end{bmatrix},\quad B_2=\begin{bmatrix}1629842.00\\ -5270.75\end{bmatrix}$$
$$C_2=\begin{bmatrix}0.0192 & 0.9906\end{bmatrix},\quad D_2=-0.1265$$

Boost Mode:

$$A_3=\begin{bmatrix}-3924.53 & -31446.54\\ 786.16 & -393.08\end{bmatrix},\quad B_3=\begin{bmatrix}848716.98\\ -10400.94\end{bmatrix}$$
$$C_3=\begin{bmatrix}0.0189 & 0.9906\end{bmatrix},\quad D=-0.2496$$

For mean square stability analysis of the power converter system, we convert the system to discrete time domain and model the system as a Markov jump linear system [9] with three operation modes as

$$G:\ \begin{cases}x[k+1]=A_{\theta[k]}x[k]+B_{\theta[k]}u[k]\\ y[k]=C_{\theta[k]}x[k]+D_{\theta[k]}u[k]\\ x[0]=x_0,\ \theta[0]=\theta_0\end{cases} \tag{8}$$

where $\theta[k]\in\{1,2,3\}$ stands for a stationary Markov chain, the system parameters $A_{\theta[k]}$, $B_{\theta[k]}$, $C_{\theta[k]}$, and $D_{\theta[k]}$ are changing with $\theta[k]$. The transition probability between all modes is described as matrix $P=\begin{bmatrix}p_{ij}\end{bmatrix}_{3\times3}$, $i,j\in\{1,2,3\}$, $p_{ij}\ge0$ and $\forall i,\ \sum_{j=1}^{3}p_{ij}=1$. The Markov jump system (8) is mean square stable if and only if there exists a collection of positive definite matrices X_1, X_2, X_3, such that the

following LMI is satisfied.

$$\forall i \in \{1,2,3\}, \qquad A_i^T \left(\sum_{j=1}^{3} p_{ij} X_i \right) A_i - X_i < 0 \qquad (9)$$

The Markov jump system and its mean square stability conditions are depicted in Figure 9.

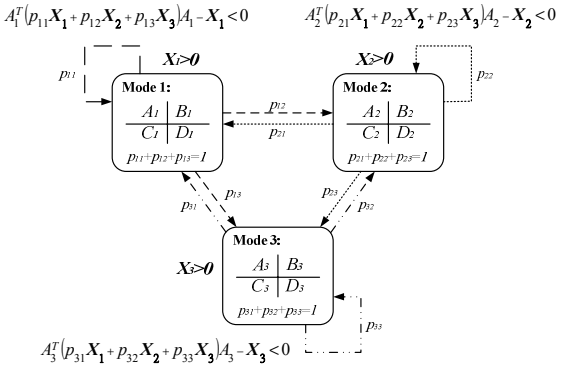

Figure 9. Markov Jump Linear System with three Operation Modes

In this design, the following probability transition matrix P is selected to proceed to the mean square stability analysis.

$$P = \begin{bmatrix} 0.9 & 0.1 & 0 \\ 0.2 & 0.6 & 0.2 \\ 0 & 0.3 & 0.7 \end{bmatrix} \qquad (10)$$

The results show that the jump systems are mean square stable. However, we should bear in mind that the stability margins of the buck-boost converter system depend on the system parameters (inductor and capacitor values, the load current, etc.). The system shall be designed to provide good stability margins for each individual operation mode and to guarantee the mean square stability of the jump system.

V. BATTERY MANAGEMENT APPLICATION

The purposes of the battery management system are to monitor and control the storage and delivery of the energy drew from the solar panels. The primary goal is to maximize the utility of the available solar power. Due to the possible rapid variations of the atmosphere conditions or the incident angles of sunlight, the supply voltage from the solar panel can be higher or lower than the required voltage for charging the batteries. To facilitate the maximization of the utilization of the available solar power, the buck-boost power converter discussed in the previous sections is incorporated in the battery management system. The functional block diagram of the battery management system is shown in Figure 10. The battery management system consists of an auto-ranging power converter, a relay and battery modules and a charge controller. The auto-ranging power converter is an LTC3780 buck-boost controller based buck-boost power converter. Two Lithium ion (Li-ion) polymer rechargeable battery (HECELL, battery model: H6849D5-4800mAh) modules are included in the system. One is for charging module and the other one is for discharging modules. Each module contains two sub-modules. A battery sub-module consists of three Li-ion battery cells. The construction of the relay and battery modules is depicted in Figure 11. In Figure 11, BAT-1 and BAT-2 form the charging module while BAT-3 and BAT-4 serve as the discharging module. The charge controller controls the charge and discharge of the batteries. In charging process, the constant current followed by constant voltage scheme is implemented. The battery sub-modules are charged sequentially. The constant current/constant voltage control circuitry is shown in Figure 12. The charging process is as follows. We first select the battery to be charged through the battery selection command from the PIC microcontroller. Then set the constant current selection and control commands to initiate the constant current charging mode. The charge current for constant current charging mode is

$$I = \frac{V_F}{R_S}\left(\frac{R_2 + R_3}{R_1 + R_2 + R_3} \right) \qquad (11)$$

where R_S is a small resistor connected to the battery for current measurement. In this design, $R_S = 0.1\Omega$ is used. The voltage V_F at the output of the operational amplifier is fed back to the auto-ranging power converter for regulating the charge current. The voltage V_F is maintained at 0.8V through the auto-ranging regulation loop. For instance, when $R_1 = 30\text{k}\Omega$, $R_2 = 1.96\text{k}\Omega$ and $R_3 = 2.2\text{k}\Omega$ are selected, the charge current will be regulated at 1A. During the constant current charging process, we continuously monitor the terminal voltage of the battery. When the battery voltage reaches the predetermined voltage level, the charging mode will be switched from constant current to constant voltage mode. For constant voltage charging, the divided charge voltage V_{CV} is fed back to the auto-ranging power converter to regulate the charge voltage to a preset voltage level. The charging process will be terminated when the battery voltage reaches its voltage limit. After completion of the charge cycle, we will switch to the second battery sub-module and repeat the charging process. When the battery sub-modules in the charging module are fully charged, we may exchange the charging and discharging modules to continue to supply power to the loading systems.

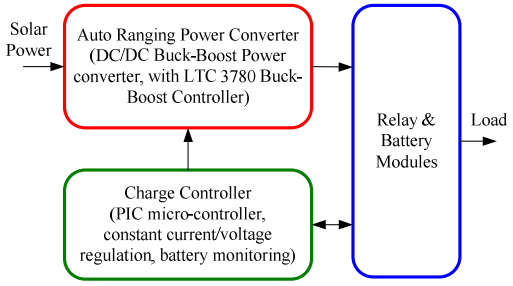

Figure 10. Functional block diagram of the battery management system

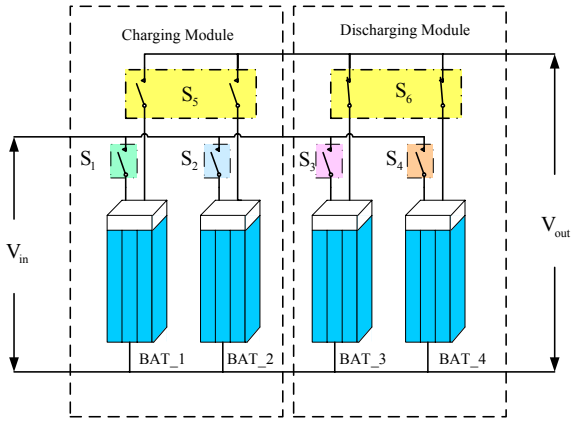

Figure 11. Li-ion battery modules and relay control structure

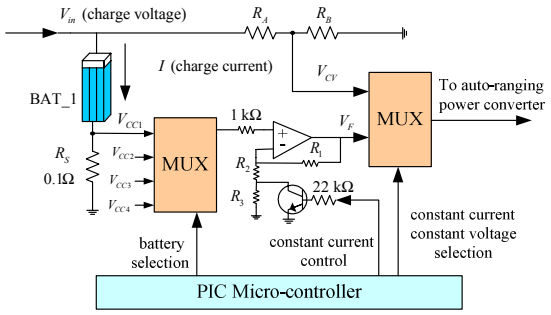

Figure 12. Constant current/ voltage control circuitry

VI. CONCLUSION

In this study, we discuss the small signal stability of a non-inverting synchronous buck-boost DC/DC power converter for a solar power management system. The system can operate in buck, buck-boost or boost mode according to the condition of the supply voltage. The stability margins of each individual operation mode for different system parameters including the inductor and capacitor values, supply voltages and load conditions are analyzed. The stability margins depend on the system parameters and the load conditions. Stability margins can be improved by the increasing capacitor value or decreasing the inductor value as long as they are within the design limitations. The system will jump among the buck, buck-boost, and boost modes of operation due to the variations of the supply voltage. A Markov jump linear system is modeled to evaluate the mean square stability of the system. With careful selection of the system parameters, we can achieve adequate small signal stability margins of each individual operation mode and mean square stability of the jump system. Application of the buck-boost power converter to a solar power battery management system is also discussed in the paper. With the incorporation of the buck-boost converter, we may maximize the utility of the available solar power drawn from the solar panel.

REFERENCES

[1] Duarte, J. L., Wijntjens, J. A. A., and Rozenboom, J., "Designing light sources for solar-powered systems". *Proc. 5th European conf. Power Electronics and Application*, vol. 8, 1993. p. 78–82.

[2] Hermann, U, and Langer, H. G., "Low-cost DC to AC converter for photovoltaic power conversion in residential applications". *Proc. IEEE PESC'93*, June 1993. p. 588–94.

[3] Bose, B. K., Szczesny, P. M., and Steigerward, R. L., "Microcomputer control of a residential photovoltaic-power conditioning system". *IEEE Trans Ind Applicat* 1985; IA-20:1182–91.

[4] Shiau, J.-K., Ma, D.-M., Yang, P.-Y., Wang, G.-F., and Gong, J.-H., "Design of a Solar Power Management System for an Experimental UAV", *IEEE Transactions on Aerospace and Electronic Systems*, to appear.

[5] Weissbach, R. S., and Torres, K. M., "A Non-inverting Buck-Boost Converter with Reduced Components Using a Microcontroller". *SoutheastCon, 2001. Proceedings. IEEE, 30 March-1 April 2001* pp.79-84

[6] Sahu B., and Rincon-Mora, G.A, "A Low Voltage, Dynamic, Noninverting, Synchronous Buck-Boost Converter for Portable Application", *IEEE Transactions on Power Electronics*, 2004, Vol. 19, No.2,: pp. 443-452.

[7] Gaboriault, M., and Notman, A., "A High Efficiency, Non-Inverting, Buck-Boost DC-DC Converter", *Applied Power Electronics Conference and Exposition, 2004. APEC'04. Niniteenth Annual IEEE* ,vol.3 ,pp. 1411-1415.

[8] Qiao, H., Zhang, Y., Yao, Y., and Wei, L., "Analysis of Buck-Boost Converter for Fuel Cell Electric Vehicles". *IEEE International Conference on Vehicular Electronics and Safety, 13-15 DEC. 2006,* pp.109-113.

[9] Costa, O. L. V., Fragoso, M. D., and Marques, R. P., *Discrete-Time Markov Jump Systems*, Springer-Verlag, London, 2005.